

# Coring damage mechanism of the Yan-tang group marble: combined effect of stress redistribution and rock structure

Peng Yan<sup>1,2</sup> · Wenbo Lu<sup>1,2</sup> · Yanli He<sup>1,2</sup> · Wei Zhou<sup>1,2</sup> · Ming Chen<sup>1,2</sup> · Gaohui Wang<sup>1,2</sup>

Received: 6 September 2015 / Accepted: 13 December 2015 / Published online: 29 December 2015  
© Springer-Verlag Berlin Heidelberg 2015

**Abstract** Micro-cracks induced by the coring process in rock samples retrieved from high in situ stress conditions may seriously influence the evaluation of rock properties. This paper presents work performed to study the coring damage mechanism of marble samples containing a kind of inclined grey (or brown) ribbon-like stripes, whose mineral components are calcite and dolomite. These samples were obtained from the Jin-ping Second Stage Hydropower Station (JPII) in China, and the coring site is located in the strata of the 5th layer of the Yan-tang group marble in the Middle Triassic system ( $T_{2y}^5$ ). A special stress-relief coring scheme was carried out to collect rock samples under different stress levels at one position, then the coring damage in these samples was examined by sonic wave testing and acoustic emission monitoring under uniaxial loading conditions, and a numerical simulation was also conducted to investigate the stress path experienced by a rock core during sampling. The results indicate that for the specific Jin-ping Yan-tang group marble ( $T_{2y}^5$ ) sample, the coring damage can be attributed to two kinds of micro-cracks: horizontal micro-cracks induced by stress redistribution, and vertical or sub-vertical micro-cracks mainly derived along the special rock structure. The horizontal cracks, generated by the tensile stress induced during coring, are mostly trans-granular ones, and can be regarded as the

main reason for coring damage. In contrast, the vertical (or sub-vertical) micro-cracks are mainly caused by the combined effect of coring-induced high deviatoric stress and the inclined grey-brown ribbons, and it usually occurs along grain boundaries. At a relatively low stress level, the shear failure may preferentially occur along special rock structures. However, the impact of the micro-structure on cracking reduces significantly with the increase of stress level, and then the induced tensile stress may become the dominant factor leading to horizontal cracks or diskings.

**Keywords** Coring damage mechanism · Rock structure · Tensile cracks · Shear cracks · Jin-ping II Hydropower Station

## Introduction

It has been widely accepted that extracting rock cores from boreholes with large depth can lead to a significant increase of micro-cracks, generally referred to as coring damage (Martin and Stimpson 1994). In fact, a considerable amount of literature has indicated that the strength, deformability, and elastic wave velocity of rock samples drilled from high-stress conditions may be heavily decreased by coring damage (e.g., Martin and Stimpson 1994; Holt et al. 2000; Eberhardt et al. 1999). So, it is very important to research the coring damage mechanism, and also to introduce reasonable measures to control high stress-induced fracturing to some extent.

The mechanism of coring damage has been investigated since the 1960s, and the coring damage mechanism can mainly fall into two opinions: the tension-induced cracking, and the shear or compression/shear-induced cracking during sampling in highly stressed medium. For the tensile

✉ Peng Yan  
pyanwhu@whu.edu.cn

<sup>1</sup> State Key Laboratory of Water Resources and Hydropower Engineering Science, Wuhan University, Wuhan 430072, China

<sup>2</sup> Key Laboratory of Rock Mechanics in Hydraulic Structural Engineering of Ministry of Education, Wuhan University, Wuhan 430072, China

damage mechanism, Jaeger and Cook (1963) and Stacey (1982) pointed out that the clean and un-sheared fracture surfaces of coring disks indicate the tensile mechanism of coring damage. Several other researchers (e.g., Li and Schmitt 1998; Song and Haimson 1999; Kaga et al. 2003) also revealed that core diskings is fundamentally a tensile failure phenomenon. Instead, Obert and Stephenson (1965) observed that cracking and diskings are initiated by, or are completely the result of, shear stress. Holt et al. (2000) noted that a large deviatoric stress may occur during drill-out of the core, and such a stress can lead to yielding or shear failures of the rock. Moreover, the relation between the stress magnitude and coring damage has been studied by Martin and Stimpson (1994) and Lim and Martin (2010), and their results indicate that coring damage intensity increases with coring depth. Otherwise, the coring damage can also originate from many other factors, such as the drilling vibration, the contact condition between the drill-bit and rock, the micro-structure of rock cores, and so on.

Although significant progress has been achieved, there is still uncertainty about the relationship between core diskings and the rock structure required to cause coring damage or diskings (Lim and Martin 2010; Lim et al. 2012), which has not been fully considered and discussed. Only a few printed papers have addressed this problem. For example, Martin and Christiansson (1991) studied the stress-induced micro-cracks in granite samples obtained from the 240 level of the Underground Research Laboratory (URL), and found that the orientation of the micro-cracks aligned with major sub-vertical discontinuous fractures.

The Jin-ping Second Stage Hydropower Station (JPII) in China offers a good chance to study the influence of the special rock structure on coring disturbance. The construction site of the station is mainly located in marble strata (especially the 5th layer of the Yan-tang group marble of the Middle Triassic, labelled by  $T_{2y}^5$  in geology), which contains grey to brown, ribbon-like or brecciated stripes, as shown in Fig. 1. These stripes are mainly composed of calcite and dolomite, the same as marble rock. Rock cores collected by drilling in the highly stressed site at JPII project have been proved to be seriously damaged for the high stress level at depths greater than 2000 m (Zhu et al. 2010).

In order to study the damage mechanism and distribution of stress-induced micro-cracks, methods of observing the physical properties are always used to test the rock cores obtained from great depth. These methods mainly include sonic wave velocity detection, rock permeability testing and acoustic emission (AE) events monitoring (Yukutake 1992; Lockner et al. 1992). Because of high accuracy and convenient operation, the sonic wave velocity test is always used to detect the distribution of cracks or damage in rock engineering, although it can only provide

damage in terms of averages. AE monitoring allows one to perceive the sequential development of cracking, but determining the damage distribution in rock cores based on AE monitoring should be conducted during the loading process (Zhao et al. 2006).

In the present study, rock cores mainly composed of two kinds of minerals obtained in deep tunnels in JPII project are tested to investigate the coring damage mechanism, especially the influence of rock structure on coring-induced cracking. Firstly, a special stress relief coring scheme (Shan et al. 2010) was used to collect rock samples under two different stress levels at one position. Then these samples were examined by sonic wave velocity detection and AE monitoring under uniaxial loading conditions, and a numerical simulation was also conducted to examine the stress paths experienced by rock cores during sampling.

## Sample collection

### Engineering geology

JPII, one of the largest hydropower stations built in China, is located on the Yalong River in the Sichuan Province. The most outstanding character of this project is that 4 headrace tunnels, each approximately 16.7 km in length running parallel to each other, were designed to cut through the Jin-ping Mountain. These headrace tunnels generally have an overburden depth of 1500–2000 m and a maximum depth of 2525 m.

The coring sites are located in the test tunnel excavated between the #2 and #3 headrace tunnel of the JPII project, as shown in Fig. 2. The lithology formation along the tunnel axis mainly includes: the Lower Triassic system ( $T_1$ ), the Middle Triassic system ( $T_2$ ) and the Upper Triassic system ( $T_3$ ). The Middle Triassic system ( $T_2$ ) is composed of carbonate rocks containing the Yan-tang group marble ( $T_{2y}$ ), Bai-shan group marble ( $T_{2b}$ ), Za-gu-nao group marble ( $T_{2z}$ ), and, further in, the  $T_{2y}$  marble includes several sub-groups, the 4th–6th layers ( $T_{2y}^4$ – $T_{2y}^6$ ) (Gong et al. 2012).

The buried depth of the sampling position is approximately 1900 m (as shown in Fig. 2), and the monitored in situ stress tensor is:  $\sigma_1 = 50.8$  MPa,  $\sigma_2 = 43.9$  MPa,  $\sigma_3 = 38.5$  MPa. The azimuth angle of the maximum principal stress ( $\sigma_1$ ) is primarily within the range of 120–160° (nearly parallel to the tunnel axis), and the maximum and intermediate ( $\sigma_2$ ) principal stresses are both nearly horizontal with very small dip angles (both within 5–10°), while the orientation of the minimum principal stress ( $\sigma_3$ ) is generally vertical with a dip angle of 77° (Chu et al. 2010). The rocks surrounding the test tunnel are Yan-tang group marble ( $T_{2y}^5$ ) of class III, whose geological

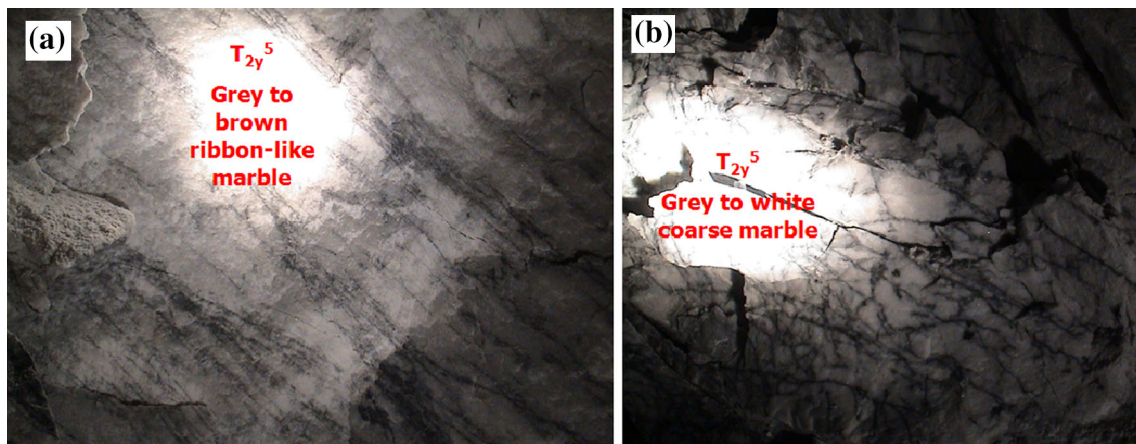
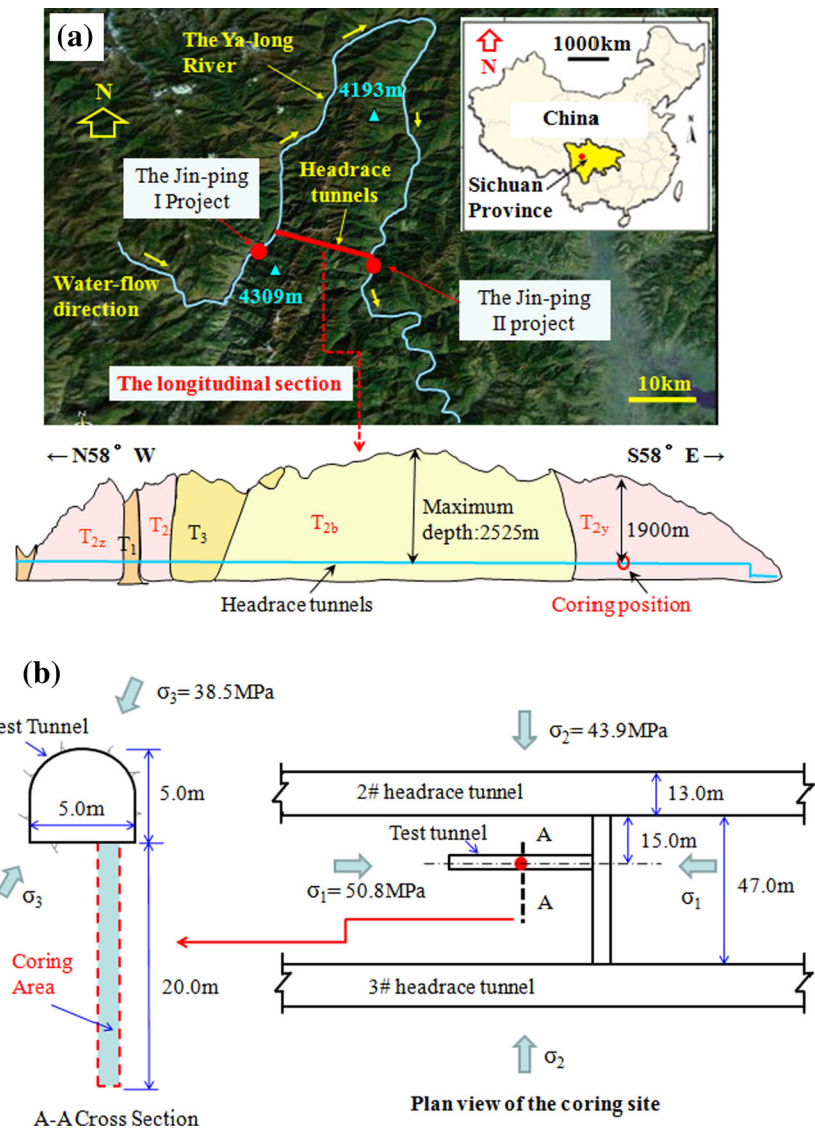


**Fig. 1** Different rock structures of the  $T_{2y}^5$  marble (the 5th layer of the Yan-tang group marble of the Middle Triassic), **a** grey to brown ribbon-like marble, **b** grey to white coarse marble

**Fig. 2** General geological conditions, **a** location of coring site and sampling arrangement,  $T_1$  means gray-green epidote and chlorite schist;  $T_{2y}$ ,  $T_{2b}$  and  $T_{2z}$  represent the Yan-tang group marble, Bai-shan group marble and Za-gu-nao group marble, respectively;  $T_3$  means sandstone and slate. The Yan-tang group ( $T_{2y}$ ) includes three sub-groups: the 4th–6th layer ( $T_{2y}^4$ – $T_{2y}^6$ ); **b** situation of the sampling position and in situ stress



strength index (GSI) is about 60–80, and the unconfined uniaxial compressive strength (UCS) ranges from 70.0 to 110.0 MPa depending on the rock structure and its mineral composition (Shan et al. 2010; Chu et al. 2010).

In order to avoid impacting the stress state of the coring area via excavation of the test tunnel, the cores were all collected from depths of 4.0–20.0 m below the test tunnel floor based on numerical simulation (Shan and Yan 2010).

### Coring scheme

A series of equally spaced de-stressing holes were drilled at a circular boundary to reduce the stress level in the central region gradually, and sampling holes are located in the circle area to collect low-stress cores. This arrangement was designed to obtain rock samples under different stress levels at the same position (Shan et al. 2010), as shown in Fig. 3.

It can be seen that there are 5 holes marked by A–E, respectively, in the middle coring area, and another 14 holes marked by Y1–Y14, respectively, lie on the circle with a diameter of 1 m. The former are referred to as coring holes, and the latter are referred to as de-stressing holes in the following text. The diameter and length of the de-stressing and coring holes are 110 mm and 15.0 m, respectively, and the clear spacing of adjacent de-stressing holes is 112.3 mm. The coring holes from A to D are arranged on the circle with a radius of 20 cm around coring hole E.

The 14 de-stressing holes were drilled firstly on the circle one by one to gradually reduce the stress in the central region. The rock samples obtained from the de-stressing holes can be considered as routine sampling under

high-stress conditions (about 40–50 MPa). The less damaged rock cores were taken from coring holes under a relatively low-stress conditions after all the de-stressing holes were completed.

A numerical model has been built to investigate the stress relief effect of the proposed sampling scheme before being implemented. The size of this model is  $3 \times 3 \times 5$  m ( $x \times y \times z$ ). The model was discrete by about 200,000 elements with a maximum size of 0.125 m. The bottom surface of the model was fixed during excavation. The stress sensor used in the simulation is the same as that mentioned above:  $\sigma_x = \sigma_1 = 50.8$  MPa,  $\sigma_y = \sigma_2 = 43.9$  MPa,  $\sigma_z = \sigma_3 = 38.5$  MPa. The principle stresses along the diameter R from the centre to the upper-right corner of the model after drilling all 14 de-stressing holes are also shown in Fig. 4.

It can be observed that in the middle region of the sampling area, the principal stresses were reduced from 40 to 50 MPa (average  $\sim 45$  MPa) to 30–38 MPa (average  $\sim 33$  MPa) after completely drilling all the de-stressing holes, and the deviatoric stress (difference between the maximum and minimum principal stresses) was reduced from 20 MPa to approximately 8 MPa. The deviatoric stress was reduced substantially, by 50 % or more, but the average principle stress was only decreased by 26.7 %. According to Holt et al. (2000), the ideal method to reduce core damage is to perform the coring operation under a low deviatoric stress condition. So, the stress relief effect of the designed sampling scheme is quite promising.

It can be inferred that if the clear distance between two adjacent de-stressing holes is reduced further, the stress relief effect may be improved. However, the drilling

**Fig. 3** Sampling scheme for obtaining cores under different stress levels at the same position

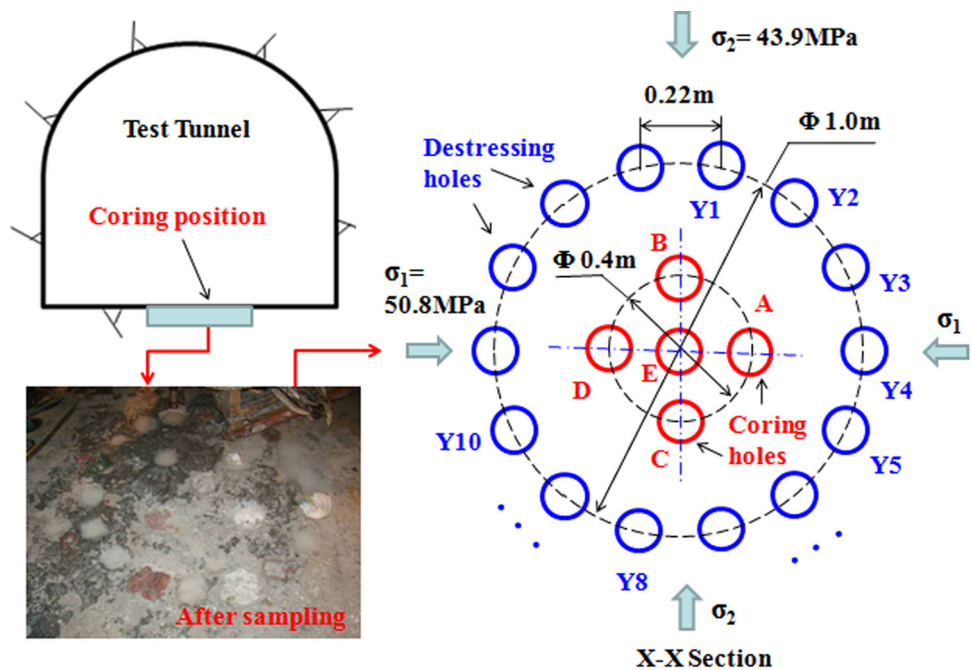
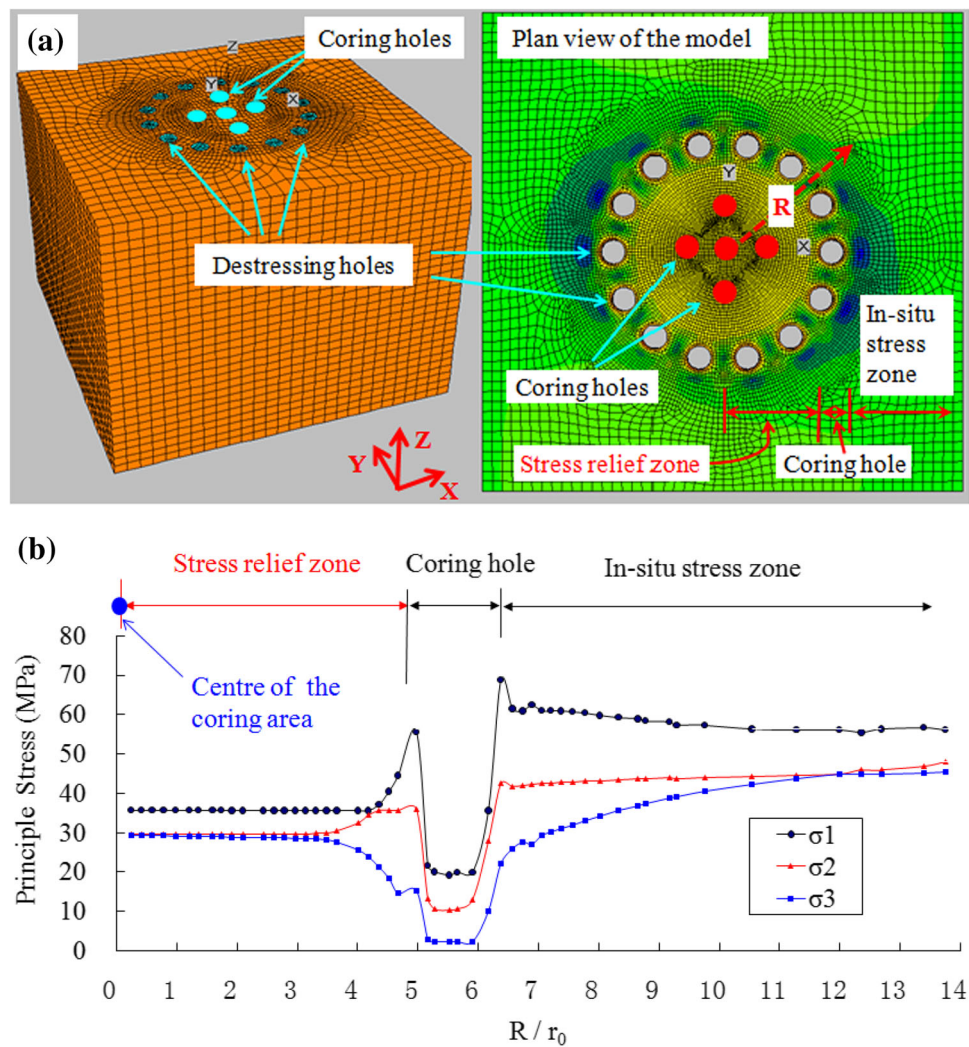




**Fig. 4** Simulation investigation of the damage-relief coring scheme, **a** numerical model; **b** simulated principal stresses on a cross-section,  $R$  is the distance from the centre of the coring area, and  $r_0$  is the diameter of the coring hole



engineer pointed out that if the clear spacing between adjacent holes is decreased to less than 100 mm, the hole-wall may be broken during drilling, leading to coring failure. The influence of hole-spacing on the stress relief effect has been discussed by Yan et al. (2012).

### Situation of rock cores

Two kinds of cores were obtained from the coring holes (referred to as low-stress cores in the following text) and de-stressing holes (referred to as high-stress cores), respectively. In total, 26 rock samples were selected to conduct the experiment, including 15 low-stress samples obtained from 2 coring holes (C and D) and 11 high-stress samples obtained from several de-stressing holes at different sampling depths. The diameter of every rock core and sample was 90 mm. Rock samples were manufactured from corresponding rock cores, and the height-diameter ratio of every rock sample was 2. The basic situations of

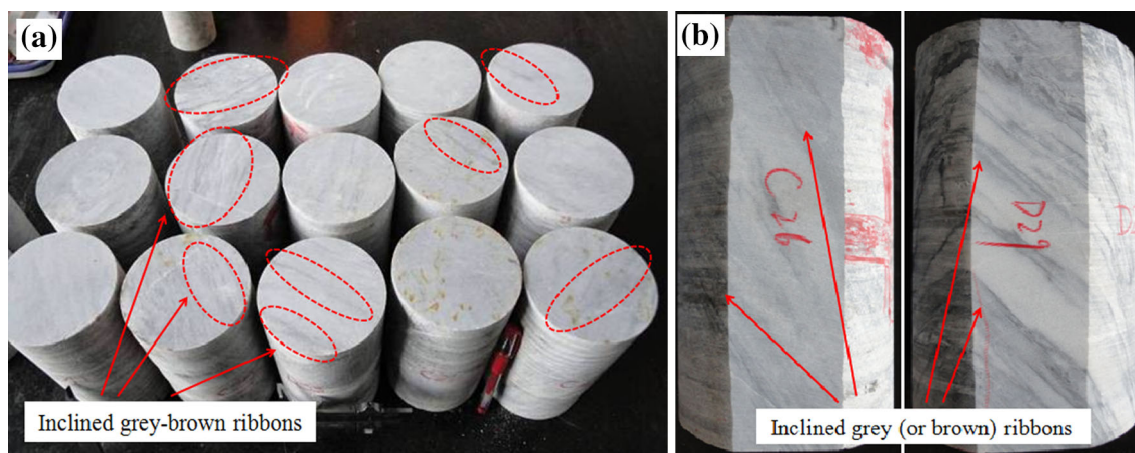
the selected samples are given in Table 1, and parts of samples are shown in Fig. 5.

It can be seen from Fig. 5 that no distinct cracks could be found on the two kinds of rock cores, excepting some grey lines of marble rock, which indicates that the coring-induced cracks or damage cannot be observed with the naked eye. More importantly, the coring direction was designed to intersect the strike plane of the grey-to-brown ribbon in the coring site with a large angle, so the inclined grey-to-brown ribbons can be detected almost in every sample. This situation may indicate that the anisotropy of these rock samples may be outstanding.

The main minerals comprising marble rock include calcite and dolomite. For the Jin-ping Yan-tang group marble ( $T_{2y}^5$ ), the estimated mineral make-up obtained through X-ray diffraction (XRD) analysis is calcite at about 54.7 % of the total quantity, and dolomite at about 45.3 %, and the grain sizes of the two kinds of minerals are 0.5–1.0 and 0.2–0.5 mm, respectively (Zhao et al. 2012).

**Table 1** Basic situation of rock cores and samples

| No. | Name of rock cores | Sampling depth (m) |       | Name of rock samples | P-wave velocity of sample (m/s) |                  |                       | P-wave velocity of hole wall (m/s) |
|-----|--------------------|--------------------|-------|----------------------|---------------------------------|------------------|-----------------------|------------------------------------|
|     |                    | Start              | End   |                      | Axial                           | Lateral-parallel | Lateral-perpendicular |                                    |
| 1   | C22                | 8.70               | 8.96  | C22-1                | 6111                            | 6056             | 5486                  | 6430                               |
| 2   | C22                | 8.96               | 9.23  | C22-2                | 6151                            | 5940             | 5361                  | 6430                               |
| 3   | C23                | 9.28               | 9.56  | C23                  | 6186                            | 5859             | 5941                  | 6418                               |
| 4   | C25                | 9.72               | 9.93  | C25-1                | 6229                            | 6047             | 5969                  | 6575                               |
| 5   | C25                | 9.93               | 10.20 | C25-2                | 6151                            | 5968             | 5435                  | 6550                               |
| 6   | C25                | 10.20              | 10.42 | C25-3                | 5855                            | 5978             | 5380                  | 6575                               |
| 7   | C26                | 10.42              | 10.82 | C26                  | 6126                            | 6103             | 5440                  | 6870                               |
| 8   | C28                | 11.17              | 11.55 | C28                  | 5621                            | 5557             | 5522                  | 6524                               |
| 9   | C30                | 11.91              | 12.21 | C30                  | 6023                            | 5697             | 5685                  | 6454                               |
| 10  | D28                | 12.20              | 12.45 | D24                  | 5947                            | 5635             | 5760                  | 6219                               |
| 11  | D29                | 13.87              | 14.17 | D29                  | 5748                            | 5540             | 5422                  | 6393                               |
| 12  | D33                | 16.83              | 17.05 | D33                  | 5754                            | 5982             | 5409                  | 6299                               |
| 13  | D38                | 18.80              | 19.05 | D38-1                | 5743                            | 5799             | 5422                  | 6220                               |
| 14  | D38                | 19.85              | 19.30 | D38-2                | 5890                            | 5944             | 5393                  | 6220                               |
| 15  | D41                | 19.80              | 20.03 | D41                  | 5450                            | 5201             | 5329                  | 6328                               |
| 16  | Y1-1               | 4.65               | 4.97  | Y1-1                 | 5918                            | 5835             | 6134                  | 6300                               |
| 17  | Y4-2               | 6.06               | 6.36  | Y4-2                 | 5954                            | 5986             | 5837                  | 6179                               |
| 18  | Y11-1              | 6.35               | 6.58  | Y11-1                | 5367                            | 5653             | 5426                  | 6400                               |
| 19  | Y11-1              | 6.59               | 6.88  | Y11-2                | 5516                            | 5438             | 5295                  | 6350                               |
| 20  | Y9-1               | 7.56               | 7.86  | Y9-1                 | 4820                            | 5006             | 5350                  | 6250                               |
| 21  | Y3-2               | 9.97               | 10.37 | Y3-2                 | 5414                            | 5324             | 5104                  | 6500                               |
| 22  | Y10-1              | 10.26              | 10.61 | Y10-1                | 5179                            | 4926             | 4285                  | 6663                               |
| 23  | Y8-2               | 11.64              | 11.96 | Y8-2                 | 5275                            | 5258             | 5258                  | 6390                               |
| 24  | Y5-2               | 17.00              | 17.20 | Y5-2-1               | 5210                            | 5407             | 5088                  | 6340                               |
| 25  | Y5-2               | 17.20              | 17.40 | Y5-2-2               | 5517                            | 5541             | 5143                  | 6300                               |
| 26  | Y2-2               | 19.92              | 20.32 | Y2-2                 | 4944                            | 5029             | 5033                  | 6321                               |

**Fig. 5** Examples of manufactured rock samples and the *brown ribbons*, **a** top review; **b** front review (after manufacturing)

### Distribution of stress-induced micro-cracks

In this section, the sonic wave velocity detection and AE monitoring are used to examine the distribution of the coring-induced micro-cracks in the Jin-ping Yan-tang group marble ( $T_{2y}^5$ ) cores, which may be influenced by the combined effects of rock structure and stress relief during sampling.

### Sonic wave velocity testing

A HX-SY02B non-metal, sonic wave detector produced by the Yue-yang Ao-cheng Technology Co., LTD. and a pair of flat sonic probes with sampling frequency ranging from 40 to 1000 kHz were used for testing.

In order to increase the contact condition (or coupling condition) between the flat sonic probe and rock sample, four small flats were produced at the ends of two orthographic diameters (the subsequent AE monitoring test also requires these flats), as shown in Fig. 6. The two pairs of orthographic diameters (marked by d1-1 & d1-2, d2-1 & d2-2, respectively), located at the H/3 from the top and bottom, respectively, were selected to test the sonic wave velocity. And d1-1 & d2-1 (blue color) and d1-2 & d2-2 (red color) are presupposed to be parallel and perpendicular to the main strike plane of grey (or brown) ribbons in every sample, as shown in Fig. 6a. The two special directions are referred to as lateral-parallel and lateral-perpendicular in the following literature.

Firstly, the axial sonic wave (P-wave) velocity was obtained by detecting it three times and calculating the average value. Then, the lateral P-wave velocities were detected three times along each of the four diameters (shown in Fig. 6), and then their average values were calculated to obtain two meaningful velocities in lateral-parallel and lateral-perpendicular directions, respectively. In addition, the P-wave velocities of the de-stressing hole wall and coring hole wall were also detected with the same sonic detecting equipment and an ordinary single-hole sonic probe.

Figure 7 presents the results of detected P-wave velocities between the two kinds of samples in all the three directions (including axial, lateral-parallel and lateral-perpendicular directions), and the axial P-wave velocity of the sampling hole wall versus hole depth is also given.

It can be seen from Fig. 7a-c that the P-wave velocities of low-stress samples at all the three detecting directions are evidently larger than that of high-stress samples at same hole-depths, which indicates that the samples retrieved from a high-stress condition (obtained from de-stressing holes with in situ stress of 40–50 MPa) are more severely damaged to that collected from a low-stress condition (obtained from coring holes with in situ stress of 30–38 MPa).

Figure 7a, b presents the comparison of P-wave velocities among the three detecting directions of low-stress and high-stress samples. It can be observed that, for the two kinds of rock samples, the differences between the axial

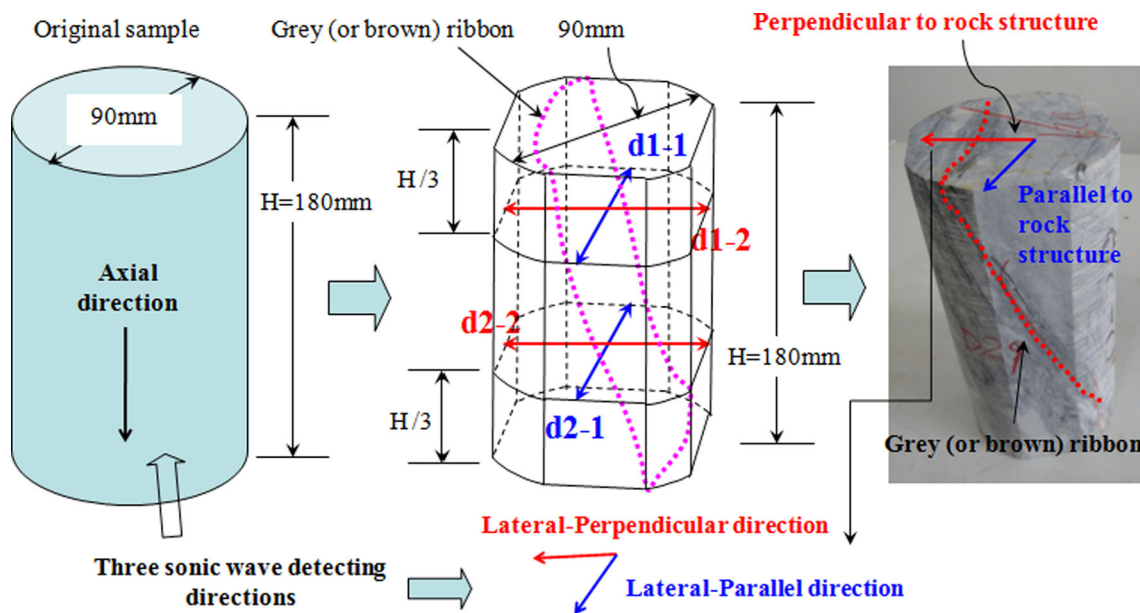
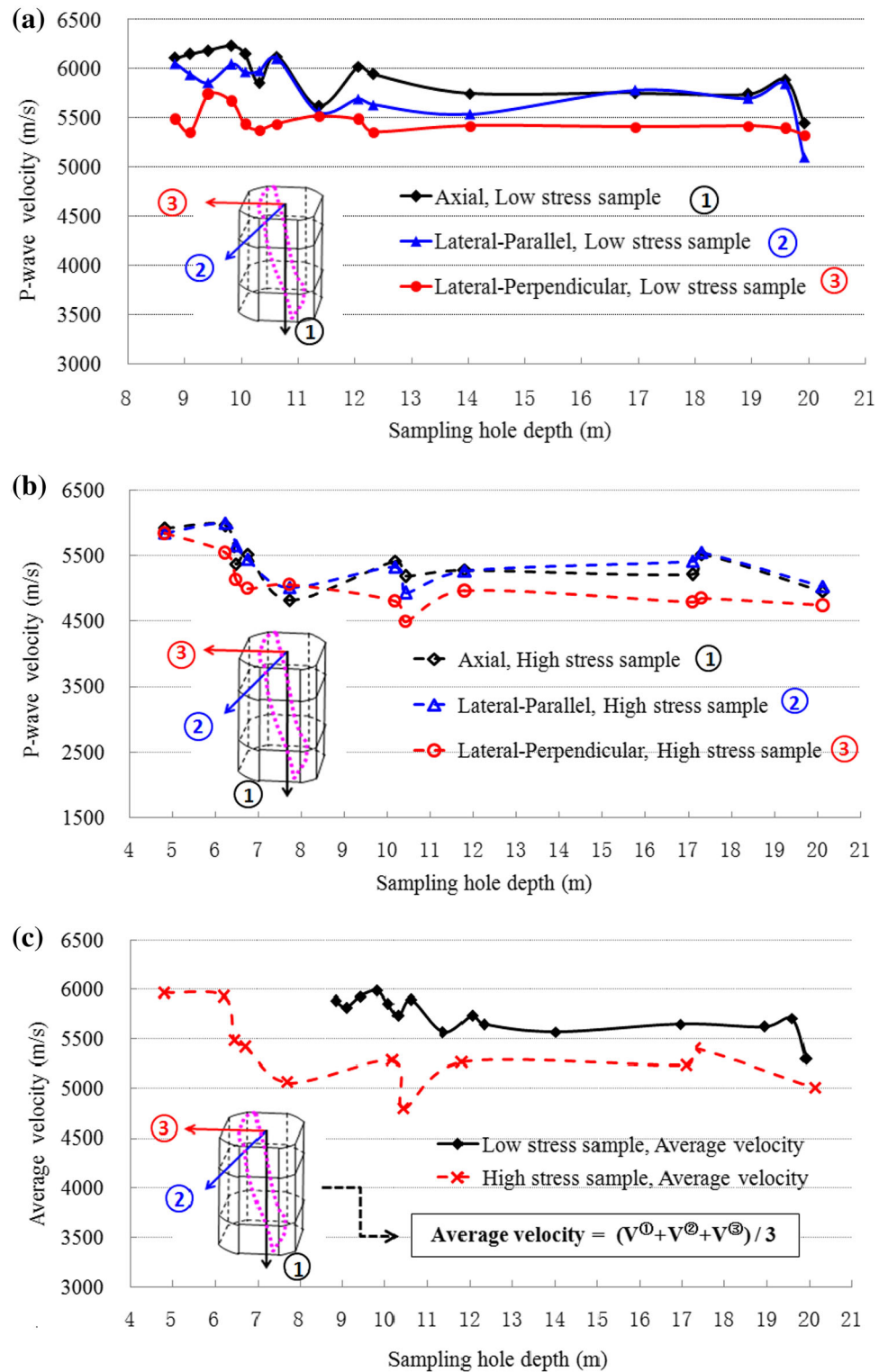


**Fig. 6** Rock sample manufacturing and P-wave detection scheme. In order to increase the contact condition between the flat sonic probe and rock sample, 4 small flats were produced at the ends of two pairs of orthographic diameters. The d1-1 & d2-1 (blue) and d1-2 & d2-2

(red) are parallel and perpendicular to the main strike plane of grey (or brown) ribbons, respectively. The two special directions are referred as lateral-parallel and lateral-perpendicular in the following literature

**Fig. 7** Results of the sonic wave velocity detection, **a, b** P-wave velocities of low-stress and high-stress samples in the three detection directions, respectively; **c** average P-wave velocity of high-stress and low-stress samples



and lateral-parallel are very small, but both of them are obviously larger than that in a lateral-perpendicular direction at most sampling depths, which indicates that the vertical or sub-vertical micro-cracks are mainly distributed parallel to the strike plane of grey (or brown) ribbons.

So, it can be preliminarily considered that the Jin-ping marble ( $T_{2y}^5$ ) sample is damaged during sampling with the generation of horizontal micro-cracks and vertical micro-cracks, and the development of vertical micro-cracks is influenced by the inclined gray stripe in the rock sample.



## Acoustic emission monitoring

The AE tests were conducted to investigate the coring damage distribution of the two kinds of rock samples. Because each micro-crack produces a transient elastic wave, the development of a cracking zone can be detected with AE testing. This technique has the advantage of sampling the whole volume in the area of interest in rock damage assessment (Yukutake 1992; Lockner et al. 1992).

The tests were carried out on a MTS815 servo-controlled rock pressure testing machine. The AE monitoring system is made by the PAC Company, and the sampling frequency of the whole system is 10 MHz with a presupposed threshold value of 100 HZ. The type of monitoring sensor is R61-AST with a working frequency range of 125 Hz–750 kHz.

In total, four samples, including two low-stress samples (D28, D41) and two high-stress samples (Y10-1, Y8-2) were selected for the AE test. The sampling depths of D28 and Y10-1 were all between 10.0 and 12.0 m (nearly at the middle of the coring holes), and the depths of D41 and Y2-2 were around 20.0 m (near the hole bottom).

The results of AE tests and corresponding stress–strain curves are shown in Fig. 8. Although much effort was made to position the AE events in the two samples, the

accuracy is not enough for the relatively small sample sizes (Zhao et al. 2006), and it is very difficult to set up more sensors. So, only the amplitudes and counts of AE events versus strain have been recorded.

As shown in Fig. 8, the AE events can be recorded through the whole loading process of the four samples, and extremely large amounts of AE events were recorded as soon as the axial force was loaded on the two high-stress samples (Y10-1 and Y2-2). This indicates that a large number of new cracks developed under a rather low-stress level (less than 30 % of the estimated UCS), below the crack initialization strength ( $\sigma_{ci}$ , the cracking initiation threshold). As the recorded AE events are mobilized when the stress level is lower than the crack initialization strength, the AE events seem not to indicate an initial cracking. Instead, the propagation of existing damages is likely to account for the generation of AEs. In other words, significant damage may exist in the specimen prior to loading (Shan et al. 2010a).

In addition, the different amounts of AE events at the early loading stage reveal that the samples retrieved from a high-stress condition (40–50 MPa) are more severely damaged to those collected from a low-stress condition (30–38 MPa), which is consistent with the results of sonic wave velocity detection. It also can be seen that the  $\sigma_{ci}$  of

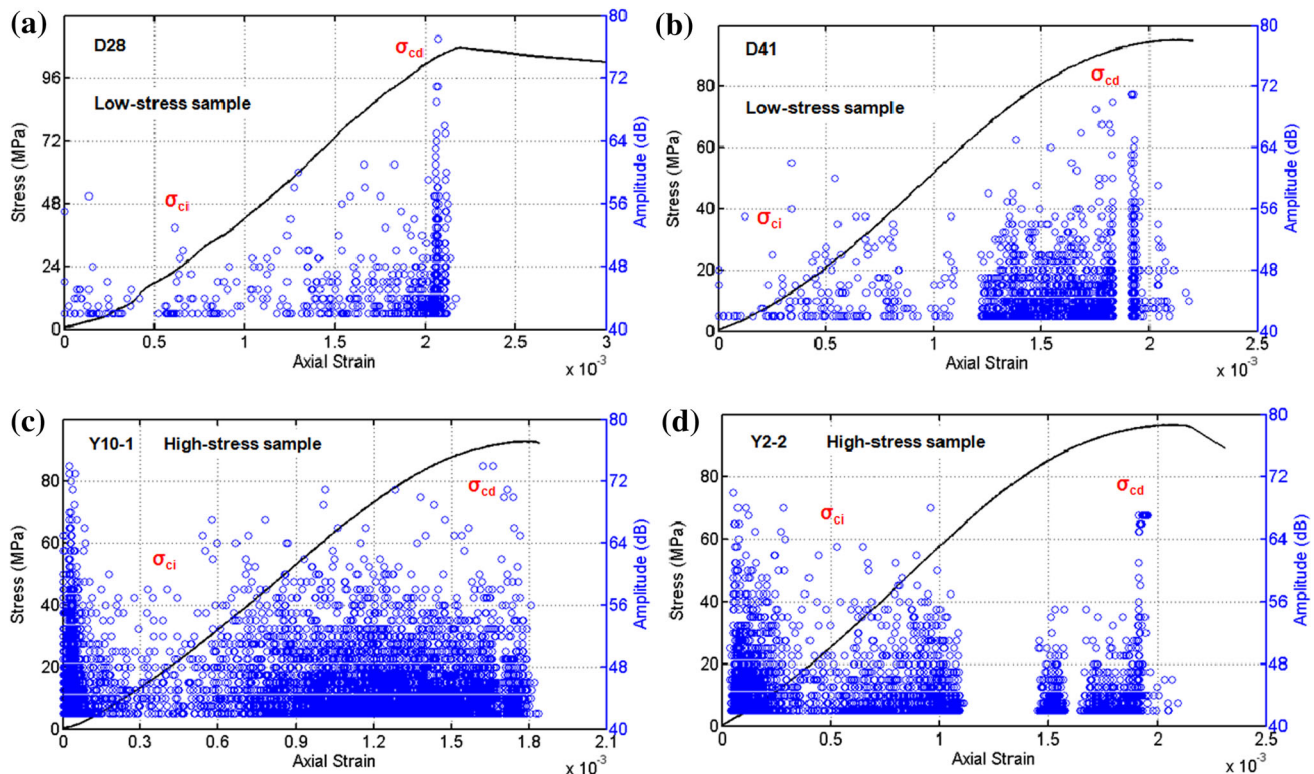
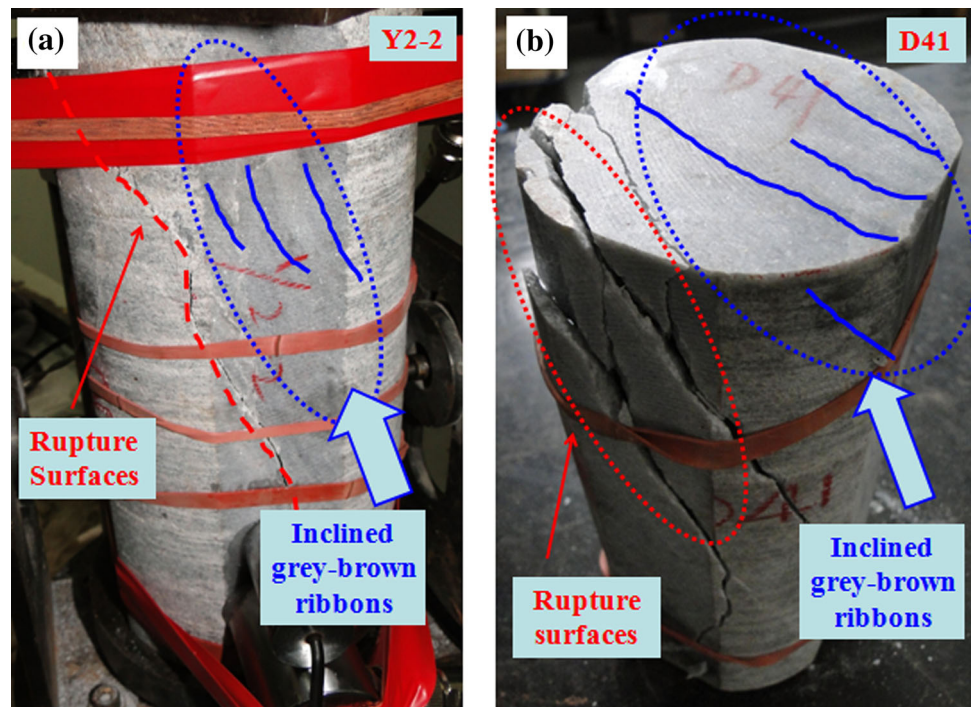


**Fig. 8** Results of uniaxial compression testing and acoustic emission monitoring. **a** D28; **b** D41; **c** Y10-1; **d** Y2-2,  $\sigma_{ci}$  and  $\sigma_{cd}$  means the cracking initiation point and cracking damage point, respectively

**Fig. 9** Failure surfaces of samples under uniaxial loading condition, **a** Y2-2; **b** D41



the 4 samples were about 20–30 MPa with an axial strain of 0.5–0.6 ‰, and their  $\sigma_{cd}$  (the cracking damage threshold) were about 70–80 MPa with an axial strain of 1.8–2.0 ‰, which indicates that the different coring damage intensity seems to have little influence on the specific mechanical parameters of the rock.

Generally, AEs result from cracking under tension. A significant amount of AE under low stress suggests the damage propagates vertically or sub-vertically in such an axial loading condition (Shan et al. 2010a). The failure surfaces of the four specimens agree well with such a suggestion. As shown in Fig. 9, the failure surfaces run through the samples in an inclined manner to indicate a shearing failure mechanism. Or, simply, the existing damages are mostly oriented more or less parallel to the implicit rock structure faces, which may be mostly determined by the existence of inclined grey-brown ribbons. Such a mechanism is not in conflict with the presumption that sub-horizontal cracks are dominant, but they have a little contribution to specimen failure under vertical loading.

The profiles of stress–axial strain curves are very close to their corresponding stress–volumetric curves at the early loading stage of the four samples, as shown in Fig. 10. This suggests that most horizontal or sub-horizontal cracks are compacted to generate a closure response under axial loading. But the strain of the axial crack compaction is very little (only about 0.5 ‰), which indicates that the amount of horizontal cracks is not very large. After the early

loading stage (about 20 MPa), the stress–volumetric curve goes in the middle of the stress–axial curve and stress–lateral curve of every sample, which reveals that the initiation and extension of horizontal (or sub-horizontal) and vertical (or sub-vertical) cracks both contribute to the volumetric strain. In other words, the coring-induced vertical (or sub-vertical) micro-cracks do, indeed, exist in the four samples as well as horizontal (or sub-horizontal) micro-cracks reported in most coring damage literature (e.g., Martin and Stimpson 1994; Eberhardt et al. 1999; Obert and Stephenson 1965; Li and Schmitt 1998; Song and Haimson 1999; Kaga et al. 2003; Holt et al. 2000). The result is also consistent with that of the P-wave detection of rock samples.

So, for Yan-tang group marble ( $T_{2y}^5$ ) samples from the JPII project, the coring damage can be attributed to two kinds of micro-cracks. The main reason for damage was horizontal micro-cracks induced by stress relief or the tensile stress caused by the coring process, according to many researchers (e.g., Li and Schmitt 1998; Song and Haimson 1999; Kaga et al. 2003), while the vertical or sub-vertical micro-cracks in Jin-ping marble samples can be attributed to the combined effect of the grey-to-brown ribbons and the stress relief process during coring. The results of electron microscope scanning of URL granite samples also indicated that most of the stress-induced micro-cracks occur along grain boundaries or micro-structure planes of a rock sample (Eberhardt et al. 1999).

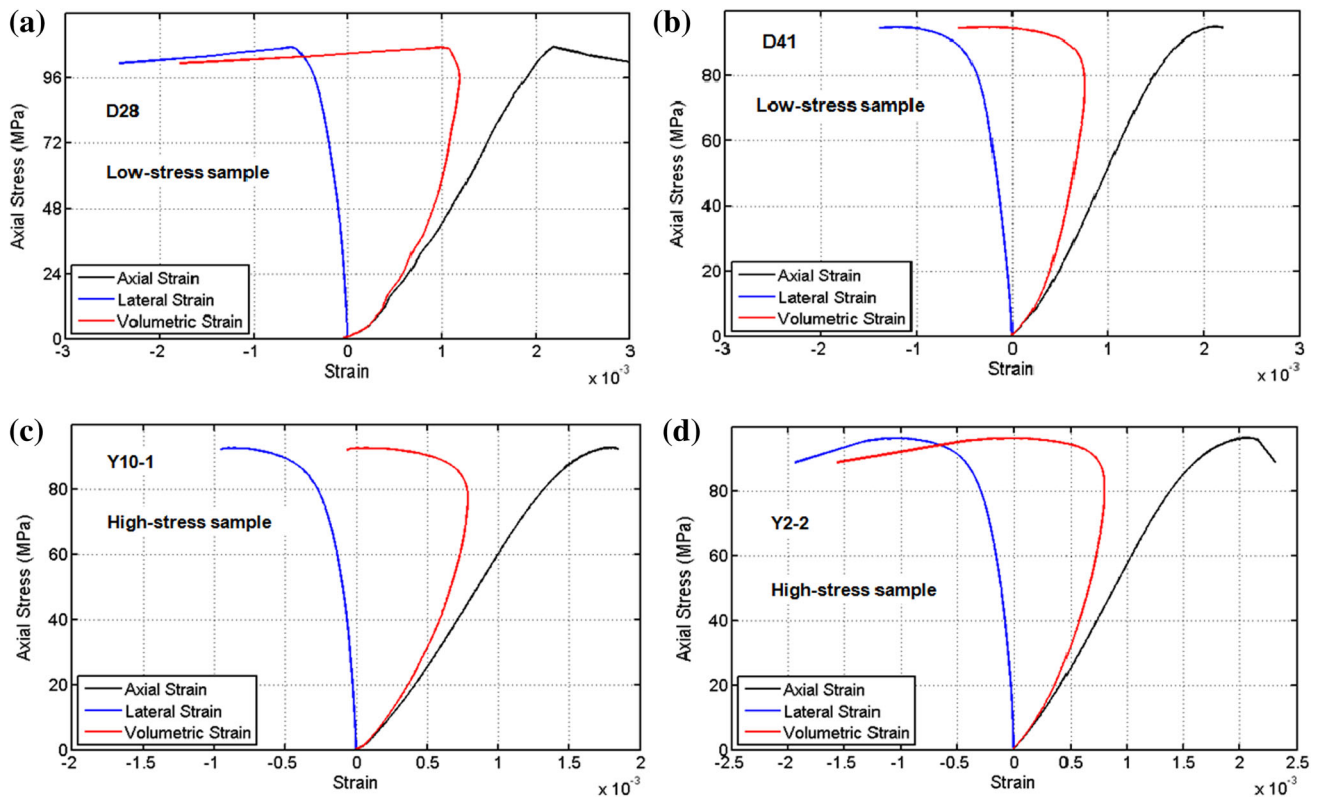


Fig. 10 Results of uniaxial compression testing and acoustic emission monitoring. a D28; b D41; c Y10-1; d Y2-2

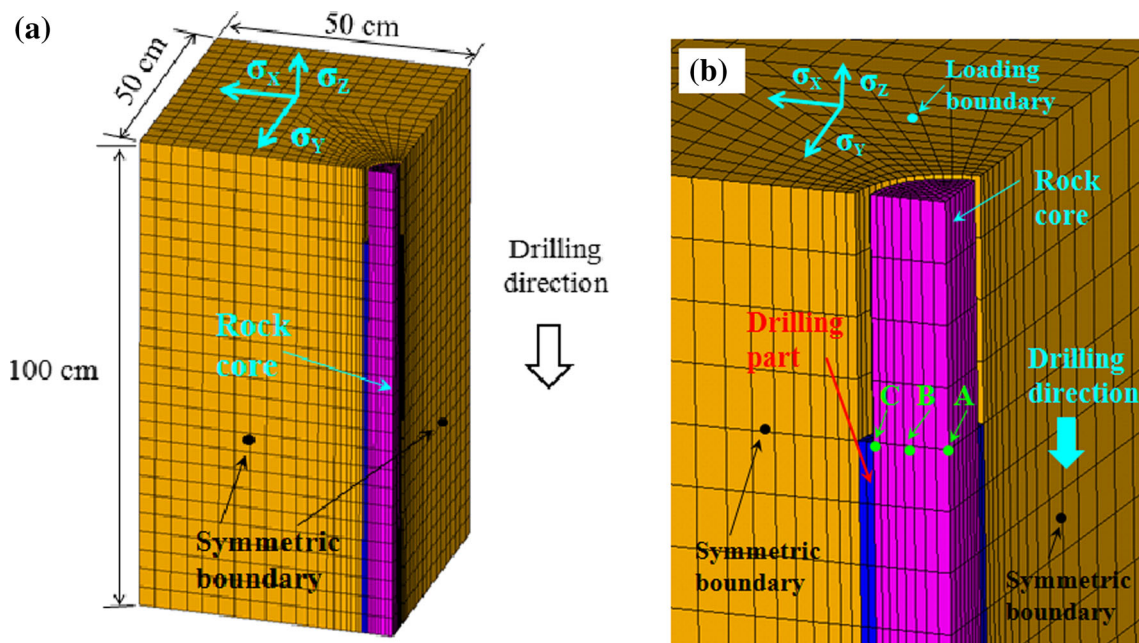


Fig. 11 Numerical model used for stress analysis, a the whole model; b the partial model



**Damage mechanism and discussion**

**Stress changes and cracking**

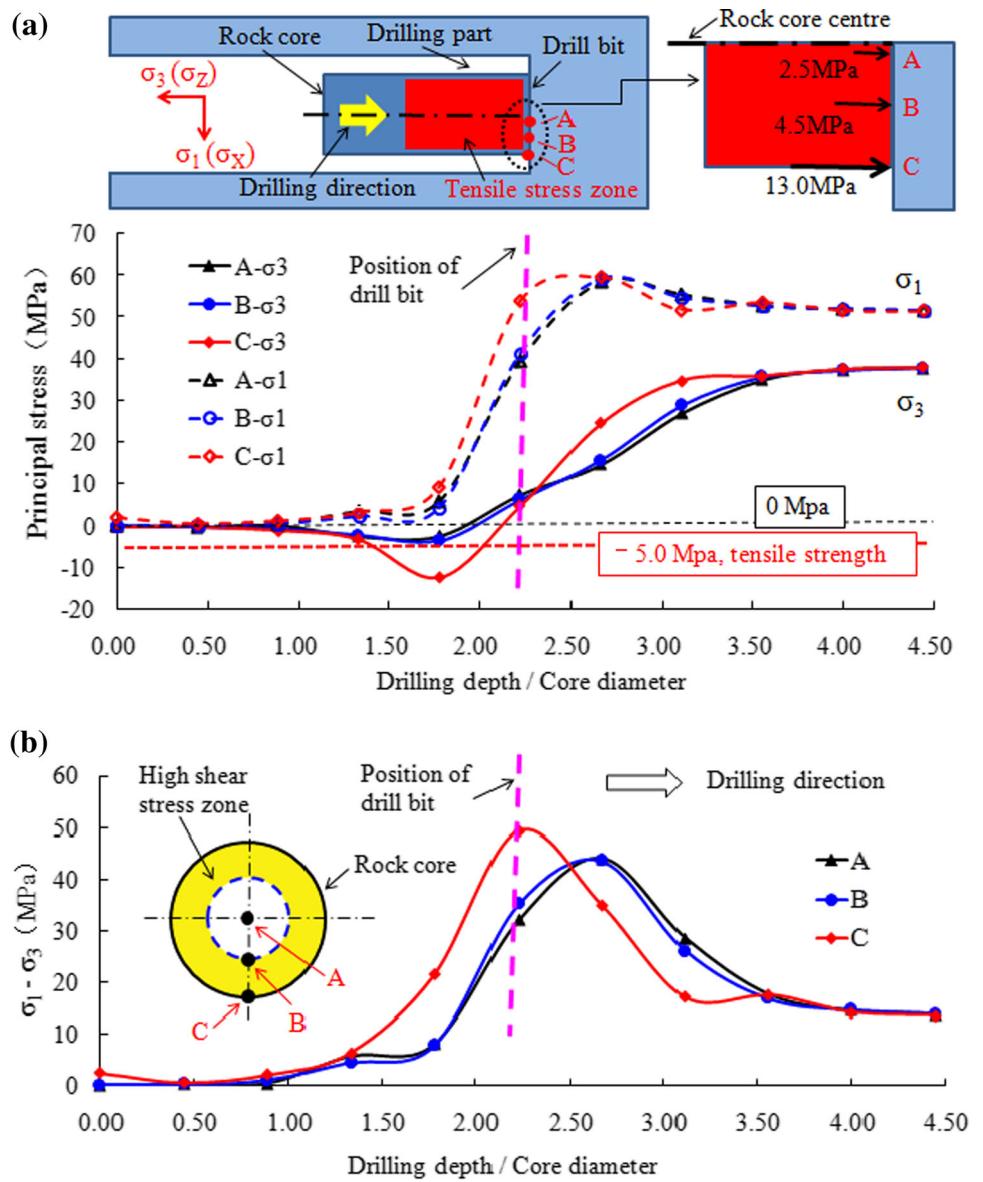
In order to verify the coring damage mechanism revealed by P-wave velocity detection and AE monitoring further, a symmetrical, elastic model was built to investigate the stress path experienced by rock cores during sampling. This was done because it is very difficult to discrete a numerical model with an enormous amount of small elements with the mineral grain size, and it also leads to huge waste of computing resources. Moreover, the mechanical characteristics of the two kinds of main mineral components (calcite and dolomite) are close to each other. So, a homogenous elastic model was established, and the analysis mainly focused on the stress changes caused by the

coring process, and the probable cracking mechanism was discussed combined with the specific rock structure of the Jin-ping Yan-tang group marble samples.

As shown in Fig. 11, the whole model includes about 12,800 elements, and the model size is  $50 \times 50 \times 100$  cm, and the diameter of the sample is 90 mm. The width of the drill bit is 10 mm. The elastic modulus and Poisson's ratio of rock mass are 30 and 0.23 GPa, respectively. The stress sensor imposed on the model is  $\sigma_x = 50.8$  MPa,  $\sigma_y = 43.9$  MPa,  $\sigma_z = 38.5$  MPa. It is applied on the three external sides of the model, and the corresponding three sides are all fixed. For every calculation step, the sampling depth is 4.0 cm.

Three points, A, B and C, located at the core centre, the middle point of core radius and the radius end on core edge, respectively, were selected to monitor the stress path experienced by the rock core, as shown in Fig. 12.

**Fig. 12** Numerical simulation results, **a** estimated principle stresses versus drilling depth; **b** estimated deviatoric stresses versus drilling depth





It can be seen from Fig. 12a that the compressive stress concentration is generated immediately below the drill bit, and no tensile stress is produced at the front of the drill bit. Once the core passes the drill bit, the compressive axial stress ( $\sigma_3$ ) turns into tensile stress, and the lateral stress ( $\sigma_1$ ) remains compressive. The maximum tensile stress occurs at the core edge (point C), and its value is about 13.0 MPa. At the middle point of the core radius (point B) and the core centre (point A), the maximum tensile stresses are 4.5 and 2.5 MPa, respectively.

The measured tensile strength of Yan-tang group marble at the JPII project is 4.0–6.0 MPa (Chu et al. 2010), and a medium value of 5.0 MPa is given in Fig. 12a. So, the tensile stress in the external part of the core is larger than the rock tensile strength, and the tensile cracks are expected to generate from the core boundary to the core centre. Furthermore, due to tensile stress ( $\sigma_3$ ) in the direction parallel to the core axis (z-axis) and the compressive stress perpendicular to the axis, the horizontal microcracks will preferentially occur in the core and expand to the core's center, then form a horizontal fracture. This coincides with the core dinking fracture

mode, and many researchers have shown that core cracking or dinking is, fundamentally, a tensile failure phenomenon (e.g., Li and Schmitt 1998; Song and Haimson 1999; Kaga et al. 2003).

In addition, Fig. 12b illustrates the principal stress difference in the core at different coring depths. It can be seen that the principal stress difference (deviatoric stress) is about 15 MPa in its original state, and it will increase to 40–50 MPa in a certain area below the drill bit, which is consistent with the results of Holt et al. (2000). The large deviatoric stress may lead to yielding and shear failures in the rock, and the Mohr–Coulomb shear failure criterion can give the best fit to this phenomenon. Considering the rock structure of Jin-ping Yan-tang marble ( $T_{2y}^5$ ), the vertical or sub-vertical cracks are generated along the grey-brown ribbons in the rock core, and are prior to cracks occurring in the external zone of the rock core due to the larger deviatoric stress around the core's edge.

So, according to the stress paths experienced by the rock core during sampling in the test tunnel at JPII, it can be considered that the Jin-ping Yan-tang group ( $T_{2y}^5$ ) marble

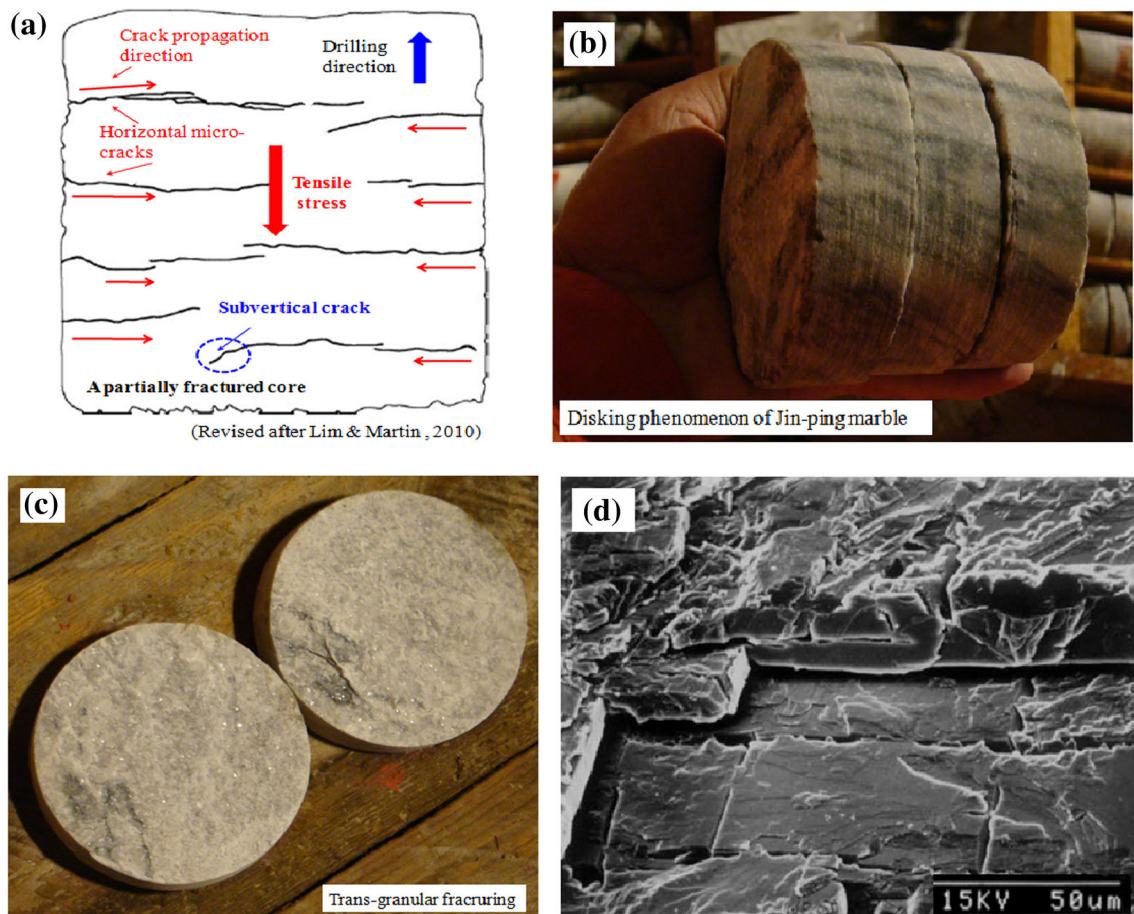


**Fig. 13** Horizontal cracks in rock cores, **a** fractures initiated and expanded horizontally; **b**, **c** disks retrieved from the de-stressing hole; **d** trans-granular fracturing

samples are mainly damaged with initiation and development of the tensile microcracks in a horizontal direction, and shearing microcracks are also produced vertically (or sub-vertically). The damage may mostly occur in the external zone of a rock sample due to higher tensile and shear stresses caused by coring in this area, while the central part of a rock sample is less damaged or undisturbed.

## Discussion

To observe the detailed characteristics of the coring-induced horizontal fracturing, partial disks were examined by cutting a core (obtained from the URL) and using a microscope and a digital camera (Lim and Martin 2010). Figure 13a shows there are clear indications that most fractures appear to have initiated and expanded horizontally. Regardless of the initiation of the fracture, the overall disk shape is relatively flat with fractures relatively uniformly spaced even when only partial diskings is observed. Since the axial tensile stress at the edge of the core is much larger than the core inside (Lim and Martin 2010), coupled with the splitting effect of horizontal compressive stress,

horizontal cracks can be considered to generate from the core's edge and propagate to the core's interior. The core diskings phenomenon can be regarded as direct evidence of horizontal tensile cracking. In addition, horizontal cracking may be mostly trans-granular fracturing (Lim et al. 2012).

A similar situation can also be observed at the coring site at JPII. Figure 13b, c presents rock disks retrieved from the de-stressing hole Y1 at a hole depth of 3.0 m (the estimated redistributed stress area caused by the test tunnel), and an electron microscope photo is also given in Fig. 13d to show the trans-granular fracturing phenomenon.

In addition, as stated by Stacey (1982), a zone of biaxial tension develops on the outer boundary of the core, leading to large extension strains, and fractures will form in a plane normal to the direction of the minor principle strain. In the zone ahead of the borehole end, these planes are generally oriented at angles 80–90° to the core axis, which can be verified by the generation of sub-vertical cracks shown in Fig. 13a. On the basis of a linear relationship between the shear strength of the rock and the lateral stress required to produce diskings at zero axial stress, Obert and Stephenson (1965) suggested that diskings is initiated by, or is

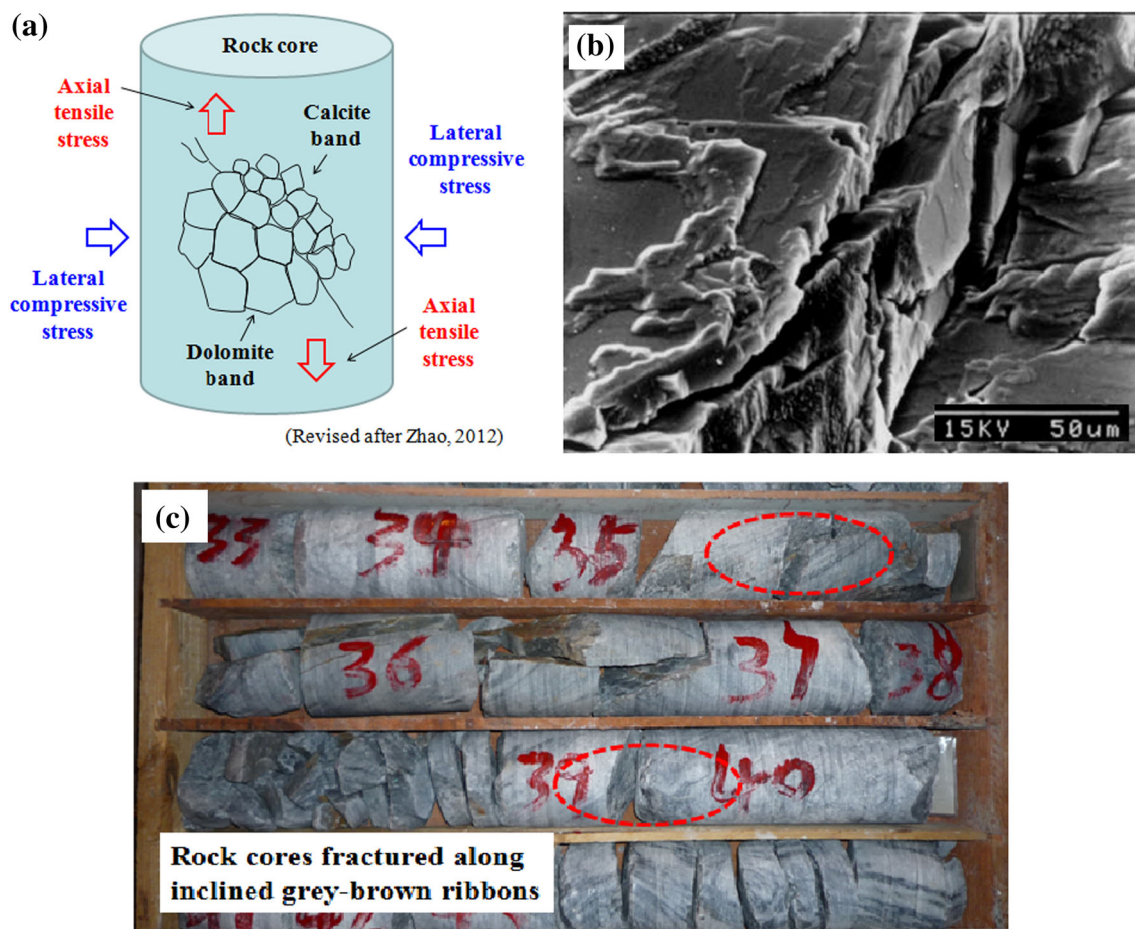


**Fig. 14** Vertical (sub-vertical) cracks in rock cores, **a** occurring mechanism of shear cracks, **b** grain boundary cracks

completely the result of, shear stress. But it appears to contradict the former author's observations of clean unsheared surfaces.

For the special rock structure of Jin-ping marble samples, vertical (sub-vertical) micro-cracks may primarily develop along the strips where different minerals connect each other, which is also confirmed by Zhao et al. (2012), as shown in Fig. 14.

According to Zhao et al. (2012), the essential reason for rock failure is the relative displacement among mineral particles making up rock, and the vertical or sub-vertical micro-cracks induced by the coring process are mainly grain boundary cracks. Martin and Christiansson (1991) also found that the orientation of the microcracks aligned with major sub-vertical discontinuous fractures. So, the existence of vertical (sub-vertical) micro-cracks reveals the influence of rock micro-structure on coring damage. At a relatively low stress level, the shear failure may occur under the combined effect of inclined ribbons and large deviatoric stress. With increasing stress level, the impact of the rock structure is reduced substantially, and the induced tensile stress may become the controlling factor leading to horizontal cracks.

So, it can be concluded that the coring damage is primarily determined by two factors: 1) in situ stress state and its magnitude, and 2) the special structure of a rock sample. The vertical (sub-vertical) micro-cracks detected in the rock cores obtained from JP II are due to the jointed effect of the specific rock structure (inclined grey-to-brown ribbons).

## Conclusion

The following conclusions can be drawn from the present study on the sampling damage mechanism of Jin-ping marble ( $T_{2y}^5$ ):

1. For the Yan-tang group marble ( $T_{2y}^5$ ) samples collected from the test tunnel in JP II, the coring damage can be attributed to two kinds of micro-cracks: horizontal and vertical (sub-vertical) cracks, as verified by sonic wave velocity testing and AE events monitoring presented in this paper. Also, the samples retrieved from a high-stress condition (40–50 MPa) are more severely damaged than those collected from a low-stress condition (30–38 MPa).
2. The horizontal or circumferential micro-cracks are mainly caused by the tensile stress generated immediately below the drill bit from the core edge to the core centre during the coring process, while the axial or sub-axial (vertical or sub-vertical, respectively) cracks can be regarded as the combined effect of coring-induced high deviatoric stress and sample structure (or inclined defects).

3. The horizontal cracking may be mostly trans-granular fracturing, while vertical (or sub-vertical) micro-cracks are mainly grain boundary cracks. At a relatively low stress level, shear failure may occur under the combined effect of inclined ribbons and large deviatoric stress. With an increase of stress level, the impact of rock structure is reduced significantly, and the induced tensile stress may become the controlling factor leading to horizontal cracks.

**Acknowledgments** This work is supported by the Chinese National Science Fund for Distinguished Young Scholars (No. 51125037) and the Chinese National Natural Science Foundation (Nos. 51179138, 51279135, 51279146 and 51009013). The authors sincerely express their thanks to all the supporters.

## References

- Chu WJ, Zhang CS, Li LQ et al (2010) Lab test of brittle behavior of marble sampled at great depth of Jinping II hydropower project. In: 44th US rock mechanics symposium and 5th US-Canada rock mechanics symposium. American Rock Mechanics Association
- Eberhardt E, Stead D, Stimpson B (1999) Effects of sample disturbance on the stress-induced microfracturing characteristics of brittle rock. *Can Geotech J* 36(2):239–250
- Gong QM, Yin LJ, Wu SY et al (2012) Rock burst and slabbing failure and its influence on TBM excavation at headrace tunnels in Jinping II hydropower station. *Eng Geol* 124:98–108
- Holt RM, Brignoli M, Kenter CJ (2000) Core quality: quantification of coring-induced rock alteration. *Int J Rock Mech Min Sci* 37(6):889–907
- Jaeger JC, Cook NGW (1963) Pinching off and diskings of rocks. *J Geophys Res* 68(6):1759–1765
- Kaga N, Matsuki K, Sakaguchi K (2003) The in situ stress states associated with core diskings estimated by analysis of principal tensile stress. *Int J Rock Mech Min Sci* 40(5):653–665
- Li Y, Schmitt DR (1998) Drilling-induced core fractures and in situ stress (1978–2012). *J Geophys Res Solid Earth* 103(3): 5225–5239
- Lim SS, Martin CD (2010) Core diskings and its relationship with stress magnitude for Lac du Bonnet granite. *Int J Rock Mech Min Sci* 47(2):254–264
- Lim SS, Martin CD, Akesson U (2012) In-situ stress and microcracking in granite cores with depth. *Eng Geol* 147:2:1–13
- Lockner DA, Byerlee JD, Kuksenko V et al (1992) Observations of quasistatic fault growth from acoustic emissions. *Int Geophys* 51:3–31
- Martin CD, Christiansson R (1991) Overcoring in highly stressed granite—the influence of microcracking. *Int J Rock Mech Min Sci* 28(1):53–70
- Martin CD, Stimpson B (1994) The effect of sample disturbance on laboratory properties of Lac du Bonnet granite. *Can Geotech J* 31(5):692–702
- Obert L, Stephenson DE (1965) Stress conditions under which core discing occurs. *Soc Min Eng* 232(3):227–235
- Shan ZG, Yan P (2010) Management of rock bursts during excavation of the deep tunnels in Jinping II hydropower station. *Bull Eng Geol Environ* 69(3):353–363

- Shan ZG, Wu XM, Yan P et al (2010) Behavior of marble at Jinping II Project—part 1: intact rock. In: Proceedings of the 44th US rock mechanics symposium, the American Rock Mechanics Association 72
- Song I, Haimson BC (1999) Core diskings in Westerly granite and its potential use for in situ stress estimation. In: Amadei B, Kranz RL, Scott GA, Smeallie PH, editors. Proceedings of 37th U.S. rock mechanics symposium, Colorado, vol 2. A.A. Balkema, Rotterdam, pp 1173–1180
- Stacey TR (1982) Contribution to the mechanism of core discing. *J S Afr Inst Min Metall* 82:269–275
- Yan P, Lu W, Chen M, Shan Z, Chen X, Zhou Y (2012) Damage-free coring technique for rock mass under high in situ stresses. *J Rock Mech Geotech Eng* 4(1):44–53
- Yukutake H (1992) Fracture nucleation process in intact rocks. *Tectonophysics* 211(1):247–257
- Zhao XD, Tang CA, Li YH, Yuan RF, Zhang JY (2006) Study on the AE activity characters under uniaxial compression loading. *Chin J Rock Mech Eng* 25(Supp. 2):3673–3678
- Zhao XP, Zuo JP, Pei JL (2012) Meso-experimental study of fracture mechanism of bedded marble in Jinping. *Chin J Rock Mech Eng* 31(3):534–542
- Zhu HC, Wu JY, Zhu YS, Zhang CS, Chen XR, Hou J, Zeng XH (2010) Rockburst at Jinping II tunneling project. In: Proceedings, 44th U.S. rock mechanics symposium/5th U.S.-Canada rock mechanics symposium (Salt Lake City, June 2010), Paper No. 10-122. ARMA, Alexandria, Virginia